Agricultural Systems 227 (2025) 104360

Contents lists available at ScienceDirect

Agricultural Systems

journal homepage: www.elsevier.com/locate/agsy

Research Paper

A crop-specific and time-variant spatial framework for characterizing rainfed wheat production environments in Ethiopia

Habtamu S. Gelagay [a,b,c,*], Louise Leroux [a,b,c], Lulseged Tamene [d], Meklit Chernet [e], Gerald Blasch [f], Degefie Tibebe [d], Wuletawu Abera [g], Tesfaye Sida [f], Kindie Tesfaye [f,h], Marc Corbeels [a,b,c], João Vasco Silva [i]

[a] AIDA, CIRAD, University of Montpellier, Montpellier, France
[b] CIRAD, UPR AIDA, 00100 Nairobi, Kenya
[c] International Institute of Tropical Agriculture (IITA), Nairobi, Kenya
[d] International Center for Tropical Agriculture (CIAT), Addis Ababa, Ethiopia
[e] Alliance of CIAT and Bioversity, Rome, Italy
[f] International Maize and Wheat Improvement Center (CIMMYT), Addis Ababa, Ethiopia
[g] International Center for Tropical Agriculture (CIAT), Accra, Ghana
[h] AGRA, Nairobi, Kenya
[i] International Maize and Wheat Improvement Center (CIMMYT), Harare, Zimbabwe

HIGHLIGHTS

- A data-driven, crop-specific framework captured spatial and temporal variability of rainfed wheat production environments.
- Crop area mapping accurately identified rainfed wheat cultivated land for 2021 and 2022
- Agro-ecological spatial units were delineated revealing five distinct wheat production environments.
- Integrating rainfed wheat area mapping with agro-ecological spatial units enabled characterization of each production environment.
- The framework is scalable and transferable to other crops and regions.

GRAPHICAL ABSTRACT

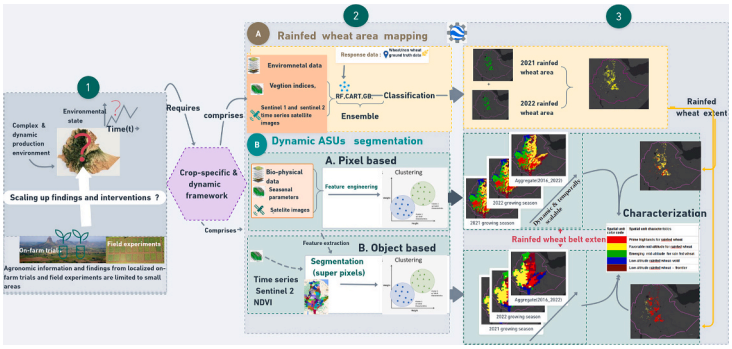

ARTICLE INFO

Editor: Jagadish Timsina

Keywords:
Crop type mapping
Spatial unit zonation
Google Earth Engine
Multi-source remote sensing

ABSTRACT

Context: Characterizing crop production environments is essential for targeted interventions, resource allocation, scaling localized findings, and agricultural decision-making. However, existing methods lack the spatial and temporal rigor required to capture spatial and temporal variability in crop production environments.
Objective: This study aimed to introduce a data-driven and dynamic spatial framework that integrates crop area mapping with the delineation of agro-ecological spatial units (ASUs) to characterize Ethiopia's rainfed wheat crop production environments.
Methods: Annual rainfed wheat areas for the 2021 and 2022 *Meher* growing seasons were mapped using an ensemble machine-learning approach, leveraging time-series satellite images and environmental data. Dynamic

* Corresponding author at: AIDA, CIRAD, University of Montpellier, Montpellier, France.
E-mail address: habtamu_sewnet.gelagay@cirad.f (H.S. Gelagay).

https://doi.org/10.1016/j.agsy.2025.104360
Received 24 January 2025; Received in revised form 18 March 2025; Accepted 23 April 2025
Available online 2 May 2025

ASUs were delineated using pixel- and object-based clustering methods, considering short-term changes (annual ASUs for 2021 and 2022) and longer-term trends (ASUs developed using data aggregated over the period 2016–2022). Clustering was based on key biophysical variables, including climatic, soil, topographic, and vegetation indices derived from satellite images that capture crop growth and development over space and time.
Results and conclusions: The framework captured the spatial and temporal variability of wheat production environments, demonstrating its scalability across space and time. Rainfed wheat area mapping across two growing seasons revealed an expansion in rainfed wheat areas, highlighting the evolving nature of rainfed wheat cultivation in Ethiopia. The integration of rainfed wheat area mapping with dynamic ASU delineation identified five main production environments for wheat in Ethiopia, allowing to better target future research and development activities toward increasing wheat productivity in the country.
Significance: The developed framework can facilitate agronomic assessments and inform the targeting of agricultural interventions, with potential applications that extend beyond this case study of rainfed wheat in Ethiopia.

1. Introduction

Characterizing production environments at a large scale is essential for informing targeted interventions, informed decision-making, and developing sustainable solutions for food security (Cassman and Grassini, 2020). However, the agronomic information derived from on-farm trials, field experiments, and crop model calibrations is mostly limited to small areas due to the substantial costs and time required to collect the necessary data (Ramirez-Villegas and Challinor, 2012; van Bussel et al., 2015; Beza et al., 2017). This limitation is accompanied by the need to account for biophysical variability across diverse agricultural landscapes (Veldkamp et al., 2001) and the difficulties in capturing temporal variability across different growing seasons (e.g., Klaus et al., 2016). A crop-specific, spatial-temporally explicit framework capable of identifying cropland cohorts with shared biophysical attributes is therefore essential. Such a framework would enable the scaling out of agronomic research for development and ensure that interventions are tailored to the distinctive characteristics of each production environment.

A notable spatial framework for characterizing crop production environments is the climatic zonation scheme of the Global Yield Gap Atlas (GYGA-CZ; van Wart et al., 2013). Other examples include the Technology Extrapolation Domain (TED) framework (Edreira et al., 2018) and the Similar Response Unit (SRU) framework (Tamene et al., 2022). Similarly, Bellón et al. (2017) and Ndao et al. (2021) contributed to related efforts using remote sensing for landscape segmentation. However, most of these efforts remain overly coarse, generic, and static, making them insufficient for effective technology targeting in complex and dynamic production landscapes. They often rely on subjective decisions when segmenting environments based on a limited set of variables. For instance, the GYGA-CZ focuses on three climatic variables, disregarding variation in edaphic factors and landscape characteristics that are essential to smallholder production systems in sub-Saharan Africa (Vanlauwe et al., 2007; Amede et al., 2022). Moreover, these frameworks are typically crop-agnostic, limiting their capacity to inform crop-specific interventions and responses to environmental conditions (Porter and Semenov, 2005). Their reliance on expert opinion-driven matrix zonation introduces subjectivity and reduces their transferability across diverse landscapes (Williams et al., 2008). Furthermore, they fail to account for inter- and intra-annual variation in environmental conditions—a crucial consideration for rainfed crop production systems.

Crop production in sub-Saharan Africa is dominated by smallholder production systems, characterized by small and fragmented farms (Giller et al., 2021; Headey et al., 2014; Fritz et al., 2015) and by heterogeneous landscapes (Kassawmar et al., 2018; Tamene et al., 2022). These farming systems are further marked by temporal shifts in crop area distribution (van Bussel et al., 2015). Spatial frameworks designed to scale out new agricultural technologies in such contexts must rely on up-to-date, fine-scale crop area distribution data (See et al., 2015; van Bussel et al., 2015), which can be derived from Earth Observation (EO) data (e.g., Wu et al., 2023; Liang et al., 2023; Ofori-Ampofo et al., 2021; Song et al., 2021; Liu et al., 2020). They should also be crop-specific and able to delineate dynamic agro-ecological zones that capture spatial-temporal variations in the production environment. Data-driven spatial frameworks leveraging multi-source and multi-thematic data are crucial in this regard given the different biophysical requirements of different crops (You et al., 2009). Such frameworks would enable the delineation of crop-specific agro-ecological spatial units (ASUs) that maximize the within-zone homogeneity while minimizing the number of zones required to encompass a specific crop area.

This study introduces and operationalizes a crop-specific and dynamic spatial framework for segmenting and characterizing heterogeneous and diverse crop production environments. The proposed spatial framework integrates high-resolution EO data, environmental datasets, and ground observations to predict crop area distribution and delineate ASUs. ASUs are defined as homogeneous spatial units that share similar biophysical conditions, within which crop production technologies are expected to perform similarly. The framework is based on three key assumptions. First, mapping the distribution of the target crop area across seasons is essential to gain insights into both spatial distribution and temporal production patterns while ensuring a balance between within-unit variability and the number of units needed to cover the targeted crop areas. Second, dynamic ASUs can effectively capture the temporal variability of crop production systems, reflecting both short-term fluctuations and longer-term trends in biophysical production potential. Lastly, integrating crop area mapping with ASUs delineation helps characterize both the current spatial distribution and the future biophysical potential of crop production. This approach leverages high spatial and temporal resolution, as well as spectrally rich satellite images (e.g., Sentinel-1 and Sentinel-2), alongside cloud computing platforms such as Google Earth Engine, to deliver precise and scalable solutions for the scaling out of agricultural technologies.

Our spatial framework was implemented for rainfed wheat production in Ethiopia. Wheat holds strategic importance for national food security in the country due to its significant import dependency (Silva et al., 2023; Tadesse et al., 2022; Senbeta and Worku, 2023). The crop is predominantly grown in highland and mid-altitude areas under rainfed conditions on soils with moderate to high productivity potential (Di Falco et al., 2007; White et al., 2001; Mersha, 2000). Effective technology targeting within Ethiopia's complex wheat production landscapes can guide investments aimed at increasing wheat productivity and resource-use efficiency in farmers' fields, where yields remain well below the biophysical potential achievable with improved agronomic practices (Silva et al., 2021). Furthermore, the framework's cost-effective design allows for its transferability to other crops and production environments, offering broader utility for agricultural research and development.

2. Materials and methods

2.1. Methodological approach

A spatial framework integrating the broader agroecological context of the Ethiopian wheat belt was developed and implemented using Google Earth Engine (Gorelick et al., 2017). The Ethiopian wheat belt encompasses both cropland and non-cropland areas that are suitable for rainfed wheat cultivation and other similar crop types (Tadesse et al., 2022; Supplementary Fig. S1). Our framework comprises three steps (Fig. 1): (1) mapping the annual rainfed wheat areas for the 2021 and 2022 *Meher* seasons (i.e., the main crop growing season from mid-June to December), which served as a foundational step by providing the spatial distribution needed for meaningful ASU delineation, (2) delineating dynamic ASUs within the Ethiopian rainfed wheat belt, and (3) integrating mapped rainfed wheat areas with ASUs to characterize the distinct rainfed wheat production environments that each ASU represents. This integration connects actual wheat distribution with the biophysical properties of ASUs, offering a comprehensive understanding of both current spatial patterns and long-term production potential. We adopted a data-driven approach allowing the data to guide the identification of spatial patterns without predefined rules (Koldasbayeva et al., 2024; Bittencourt et al., 2024) and ensuring a robust and adaptive spatial characterization of wheat production environments. Specifically, predictive machine learning techniques (Bokonda et al., 2020) were used for rainfed wheat area mapping, while pattern recognition-driven clustering approaches were applied for ASU delineation. Both approaches leveraged multi-source time-series remote sensing imagery and environmental datasets. Sections 2.2 and 2.3 detail the specific methodologies applied within this framework.

2.2. Rainfed wheat area mapping

Crop-type field data were collected during the 2021 and 2022 *Meher* growing seasons to train and evaluate models for rainfed wheat area mapping. A total of 1651 ground truth points (1251 wheat fields and 400 fields of other crops) were collected in 2021, while 2927 points (1747 wheat fields and 1180 fields of other crops) were collected in 2022. To address the class imbalance in 2021, an additional 516 non-wheat points were generated using a decision rule approach (Ghazaryan et al., 2018). This approach utilized Sentinel-2 Normalized Difference Vegetation Index (NDVI) metrics, including mean and maximum NDVI values, phase (timing of crop growth stages), and amplitude (magnitude of vegetation changes during the growth cycle) derived from NDVI time series.

Sentinel-1 and Sentinel-2 satellite images and derived variables were integrated with environmental datasets to predict the distribution of rainfed wheat areas (Fig. 1; Supplementary Table S1). Time-series information, including spectral bands, vegetation indices (e.g., NDVI), and spectral indices (e.g., greenness index) derived from Sentinel-2 satellite images, along with back-scatter coefficients derived from Sentinel-1 satellite images, was considered for the period from mid-June to late November, coinciding with the critical growth phases of rainfed wheat crops in Ethiopia. Phenology metrics, including season start and end, describing key crop growth stages, and seasonal metrics, like phase and amplitude, capturing the overall seasonal pattern of vegetation dynamics, were derived from Sentinel-2 NDVI time series. The threshold method (Jonsson and Eklundh, 2002) was used for phenology metrics, while the harmonic transformation method (Jakubauskas et al., 2001; Jakubauskas et al., 2002) was applied for seasonal metrics, respectively. Additionally, climatic variables (mean monthly precipitation, temperature, and solar radiation), soil properties (organic carbon, pH, and texture), and topographic variables (elevation and slope) were included

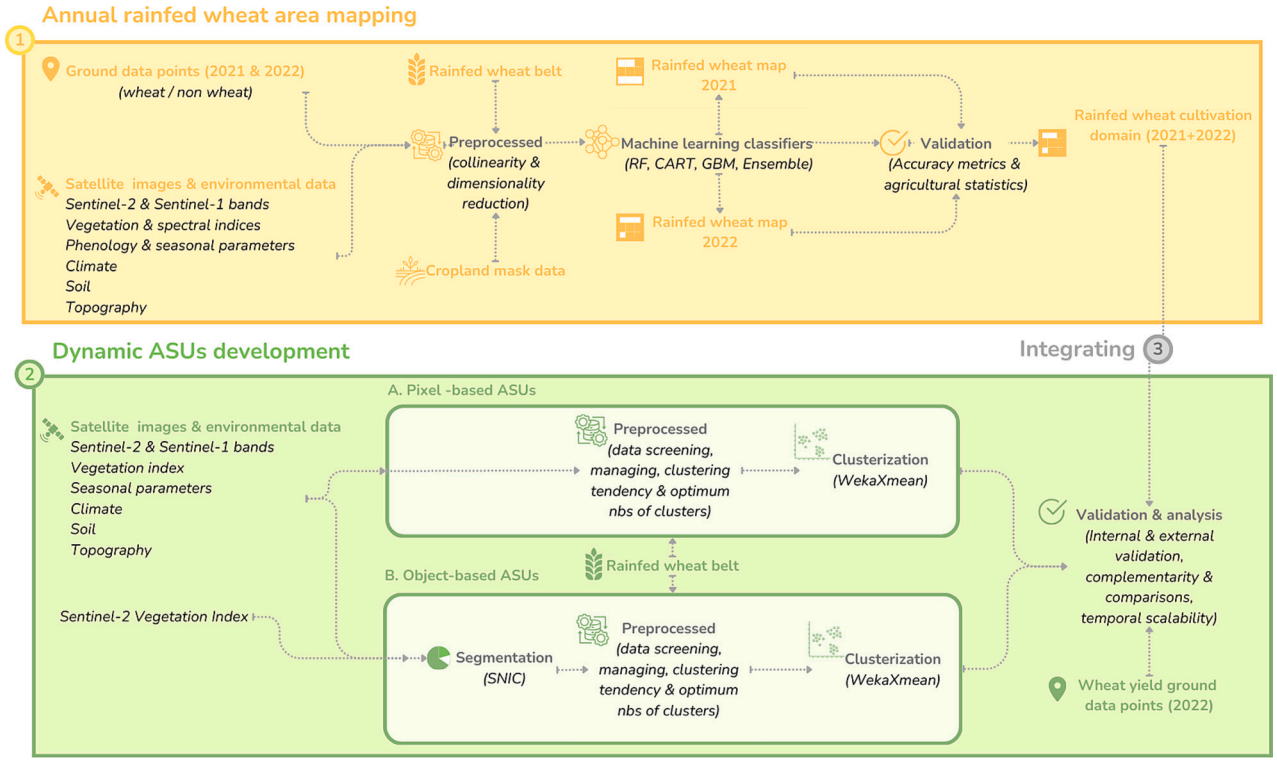

Fig. 1. | A three-step data-driven spatial framework to map the annual rainfed wheat areas, delineate agro-ecological spatial units (ASUs), and characterize rainfed wheat production environments by integrating multi-source time series satellite images and environmental data. Step 1 entails the spatial estimation of the annual rainfed wheat area. Step 2 entails the delineation of crop-specific and dynamic ASUs with two complementary approaches, pixel- and object-based clustering. Step 3 integrates the mapped rainfed wheat areas with ASUs to characterize the distinct rainfed wheat production environment that each ASU represents. RF stands for Random Forest, CART for Classification and Regression Tree, GBM for Gradient Boosting Machine, and SNIC for Simple Non-Iterative Clustering.

as predictors. All predictors were masked using a cropland mask (Zanaga et al., 2022) within the rainfed wheat belt (Supplementary Fig. S1) before model fitting. Three machine learning algorithms, namely Random Forest (RF; Breiman, 2001), Classification and Regression Tree (CART; Breimann et al., 1984), and Gradient Boosting (GB; Friedman, 2001), were trained separately for each of the 2021 and 2022 *Meher* growing seasons using 70 % of the ground truth data and evaluated on the remaining 30 %. For each growing season, the rainfed wheat maps from these models were then combined using a majority voting method (Ahmed et al., 2023), where a grid cell was classified as rainfed wheat in the final map if at least two of the three individual predictions identified it as such. The ensembled rainfed wheat area maps for the 2021 and 2022 *Meher* growing seasons were subsequently merged to capture overall spatial patterns and trends in wheat cultivation across Ethiopia.

The accuracy of the rainfed wheat distribution maps generated by each algorithm and their ensemble was assessed using the overall accuracy (OA), the producer accuracy (PA), and the user accuracy (UA) (Congalton and Green, 2019). The algorithms' generalization capabilities across different periods were also evaluated. For example, models trained on data from the 2021 *Meher* season were tested on unseen data from 2022, and vice versa. Furthermore, the estimated wheat area was compared with official statistics on harvested rainfed wheat area at national and regional levels (CSA, 2021, 2022; FAOSTAT, 2022) to ensure alignment with ground-truth data.

2.3. Delineation of dynamic agro-ecological spatial units

We segmented the rainfed wheat landscape of Ethiopia into homogeneous ASUs based on climatic, soil, topographic, and vegetation indices derived from EO data known to affect crop growth and development (Supplementary Table S1). Climatic variables included growing degree days (GDD), temperature seasonality, and aridity index as monthly averages over the growing season (van Wart et al., 2013). GDD was derived by subtracting the wheat base temperature of 2 °C (Simane et al., 1999) from the mean monthly temperatures (Muñoz Sabater, 2019). Temperature seasonality was calculated as the standard deviation of the monthly average temperature (Abatzoglou et al., 2018). The aridity index was calculated as the ratio of annual total precipitation (Funk et al., 2015) to total potential evapotranspiration (Trabucco and Zomer, 2018). Soil variables included pH (Hengl et al., 2021), and plant-available water holding capacity, estimated using the texture class-based method (Grossman and Reinsch, 2002). Elevation was included as a key topographic variable (Farr et al., 2007). Lastly, remote sensing variables such as vegetation indices, synthetic aperture radar (SAR) backscatter, and seasonal metrics, were considered to capture the spatial and temporal variability in vegetation, supporting a dynamic ASU zonation. All variables were masked to the extent of the rainfed wheat belt (Supplementary Fig. S1).

We applied a clustering approach to segment the rainfed wheat production environment into distinct ASUs, reducing intra-class variability and subjectivity in the class definition. Clustering approaches leverage distance functions to measure similarity, with smaller distances indicating higher homogeneity within groups (Cao et al., 2012; Xu and Wunsch, 2005). Two clustering approaches were implemented: pixel-based clustering, which captures fine spatial patterns, and object-based clustering, which generalizes complex patterns for broader spatial applicability. Pixel-based clustering began by analyzing the proximity distance between variables to evaluate the internal structure and clustering tendency of the data (Puzicha et al., 2000; Green and Rao, 1969). Second, the optimum number of clusters, known as ASUs in this context, was defined to: (1) capture meaningful patterns without over-simplification or excessive fragmentation, (2) establish an appropriate level of granularity, and (3) ensure that the final ASUs can support decision-making. The elbow method (Kwedlo, 2011), the silhouette coefficient (Kaufman and Rousseeuw, 2009; Rousseeuw, 1987), and the Bayesian Information Criterion (BIC, Fraley and Raftery, 1998; Gao, 2010; Neath and Cavanaugh, 2012) were used to define the optimum number of ASUs. The pixel-based clustering was conducted using the WekaXmean algorithm (Beckham et al., 2016; Arthur and Vassilvitskii, 2007), an extension of k-means clustering (Pelleg and Moore, 2000), implemented in Google Earth Engine (GEE). In contrast, object-based clustering started with super-pixel segmentation of Sentinel-2 NDVI time series (2016–2022) using the Simple Non-Iterative Clustering (SNIC) algorithm, an advanced version of Simple Linear Iterative Clustering (SLIC; Mi and Chen, 2020). This process produced super-pixels, coherent groups of grid cells (Stutz et al., 2018), from which the mean values of biophysical variables used in the pixel-based ASUs (Supplementary Table S1) were extracted. These aggregated values were then used to cluster the super-pixels using the WekaXmean algorithm, ultimately establishing object-based ASUs.

While combining pixel- and object-based clustering enables capturing the biophysical variability at different spatial scales, capturing temporal variability requires an additional step. A two-stage clustering strategy was, therefore, implemented to capture short-term variation and longer-term trends in the rainfed wheat production environment. First, year-specific biophysical attributes (Supplementary Table S1) were used to establish ASUs separately for the 2021 and 2022 growing seasons, capturing short-term variability in the production environment. Second, the same attributes, but aggregated over 2016–2022, were used to establish ASUs that reflect longer-term trends in the production environment. This two-stage clustering process was applied to both the pixel-based and object-based clustering approaches, leading to the establishment of six sets of ASUs—three from each approach.

The resulting ASUs were numerically labeled, with their spatial extent dependent on the clustering approach and the data aggregation method. Consequently, ASUs derived from different clustering methods may not correspond spatially. The ASUs from both the pixel- and object-based approaches were masked to the predicted spatial extent of Ethiopia's rainfed wheat area (Section 2.2). Finally, cumulative probability distribution functions were generated to evaluate the distribution and dynamics of ASUs across the rainfed wheat belt and the rainfed wheat area over time.

2.4. Evaluation and characterization of agro-ecological spatial units

The validity of pixel- and object-based ASUs derived from biophysical variables aggregated over the period 2016–2022 was assessed using both internal and external evaluation metrics. Internal evaluation involved the Kruskal-Wallis test (Kruskal and Wallis, 1952) to measure statistical differences in feature distributions across ASUs, assessing between-unit separability, and silhouette coefficients to evaluate within-unit cohesion (Tomasini et al., 2016). For external evaluation, wheat yield data from crop cuts conducted during the 2022 *Meher* growing season ($n = 2076$) were used. A Kruskal-Wallis test was applied to assess whether wheat yield was significantly different across ASUs. To evaluate the similarity between pixel- and object-based ASUs, proximity analysis was conducted using pairwise distance measurements (Puzicha et al., 2000). Temporal scalability and dynamism of ASUs were assessed by comparing single-year ASUs (2021 and 2022) with those derived from aggregated datasets (2016–2022) for both pixel- and object-based approaches. This was done using a pairwise distance method (Green and Rao, 1969; Puzicha et al., 2000) to capture spatial and temporal changes in the production environment.

Wheat production environments were characterized based on the estimated rainfed wheat area and the delineated ASUs, following four steps. First, pairwise similarity matrices were used to assess variable associations and identify key linking biophysical factors for clustering (Supplementary Table S1). Second, boxplot analyses were conducted to characterize each ASU based on the biophysical factors used as input (Supplementary Table S1). Third, the rainfed wheat area coverage within each ASU was analyzed to assess the extent of the current rainfed wheat production relative to biophysical conditions. Lastly, ASUs from

both clustering approaches with similar spatial configurations and biophysical characteristics were grouped for characterization and logical naming. By integrating these steps, we characterized each ASU and assigned names that reflect their suitability and potential for rainfed wheat cultivation.

3. Results

3.1. Rainfed wheat area in Ethiopia

A distinct geographical pattern was observed in the distribution of rainfed wheat areas, which were concentrated in the central region and expanded to the northern parts of Ethiopia in both growing seasons (Fig. 2A). The ensemble approach had high classification accuracy in both growing seasons, with an overall accuracy (OA) of 88 % in 2021 and 94 % in 2022 (Supplementary Table S2). The ensemble approach demonstrated strong generalizability across the two growing seasons, achieving an OA of 70 % when trained on the 2021 data and tested on the 2022 data and an OA of 90 % when trained on the 2022 data and tested on the 2021 data. Individual algorithms also performed well in identifying wheat areas, with user accuracy (UA) ranging from 92 to 96 % and producer accuracy (PA) between 95 and 97 % (Supplementary Table S2). Elevation, solar radiation, and precipitation were the most important variables in predicting the rainfed wheat crop area (Supplementary Fig. S2).

The rainfed wheat area estimated with the ensemble approach was 2.24 million hectares (M ha) in the 2021 *Meher* growing season and 2.50 M ha in the 2022 *Meher* growing season (Fig. 2D). The findings confirmed that the Oromia and Amhara regions shape the regional distribution of wheat cropland. In 2021, their combined contribution accounted for 91 % of the total rainfed wheat area at the national level, which increased to 95 % in 2022 (Fig. 2D). The estimated rainfed wheat area was 13 % larger than the official statistics in 2021 and 8 % larger in 2022. However, regional differences were notable, with the estimated wheat area closely matching official reports for Oromia and Southern Nations, Nationalities, and Peoples' (SNNP) regions, but consistently being higher for the Amhara region. For the Tigray region, the estimated rainfed wheat area aligned with the official statistics for 2021, while no official statistics were available for 2022 due to political instability in the region. The ensemble output matched the official statistics more closely than the outputs of the individual models (Supplementary Fig. S3).

3.2. Dynamic agro-ecological spatial units for rainfed wheat in Ethiopia

Pixel- and object-based clustering approaches identified five agro-ecological spatial units (ASUs 1–5), with each ASU representing a unique production environment that shares similar biophysical characteristics, where agricultural technologies are likely to perform similarly. Similar spatial patterns in ASUs were observed between pixel- and object-based clustering approaches, with stability and dynamism in their spatial patterns between the 2021 and 2022 growing seasons (Figs. 3 and 4). ASUs 3, 4, and 5 from the pixel-based approach covered about 6 %, 28 %, and 21 % of the rainfed wheat belt, respectively, and maintained consistent spatial patterns across both growing seasons, indicating stable production environments (Figs. 3A, 3C). In contrast, ASU 2 expanded in 2022, covering 27 % of the wheat belt compared to 14 % in 2021, while ASU 1 showed the opposite trend, decreasing from 39 % in 2021 to 24 % in 2022 (Fig. 3A). ASUs 1, 3, and 5 from the object-based approach also exhibited consistent spatial patterns between the two growing seasons (Figs. 3B and 3D), though there were slight variations in area coverage, particularly for ASUs 1 and 5. ASU 1 covered 24 % of the rainfed wheat belt in 2021 but decreased to 15 % in 2022, whereas ASU 5 expanded from 20 % in 2021 to 27 % in 2022. ASU 3 covered approximately 15 % of the rainfed wheat belt in both growing seasons. In contrast, ASUs 2 and 4 demonstrated changes in spatial patterns over time (Figs. 3B and 3D) but maintained nearly the same area coverage across growing seasons. ASU 4 covered approximately 19 % of the rainfed wheat belt, while ASU 2 covered around 21 % (Fig. 4D). The aggregated pixel-based ASUs 2 and 3 showed similarities in geographic extent with their corresponding ASUs in 2021 and 2022, whereas ASUs 1, 4, and 5 exhibited notable temporal changes. Conversely, the aggregated object-based ASUs showed temporal stability for ASUs 5 and 3 and temporal dynamism for ASUs 1, 2, and 4 compared to the 2022 growing season ASUs.

Pixel-based aggregated ASU 4 was identified as the dominant environment for rainfed wheat cultivation (Fig. 3G), encompassing approximately 65 % of the rainfed wheat area (Fig. 4C). Conversely, object-based ASUs 1 and 5 emerged as the primary environments, covering 43 % and 38 % of the rainfed wheat area, respectively,

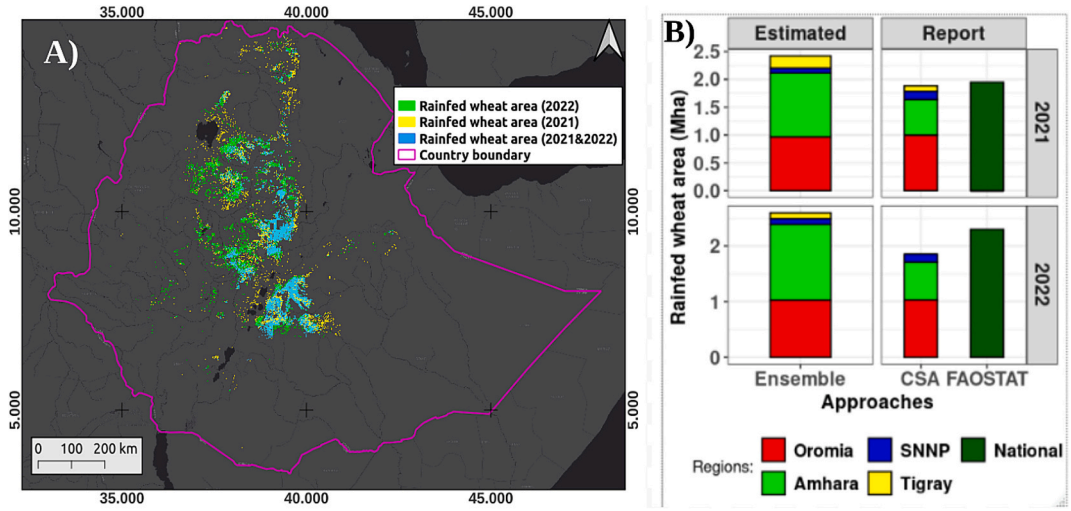

Fig. 2. | (A) Rainfed wheat area distribution for the 2021 and 2022 *Meher* growing seasons, showing wheat areas unique to each year and those identified as wheat in both years, thereby highlighting spatio-temporal patterns of wheat cultivation. (B) The rainfed wheat area estimated as the sum of the area of each grid cell (10 m × 10 m) by the total number of grid cells identified as wheat only in comparison to official statistics at regional (CSA, 2021, 2022) and national levels (FAOSTAT, 2022) for the respective growing seasons. Rainfed wheat area distribution was produced with an ensemble of gradient boosting (GB), classification and regression tree (CART), and random forest (RF). The ensemble estimation corresponds to the rainfed wheat distribution obtained from the combination of all grid cells consistently classified as wheat by at least two algorithms. Wheat area distribution estimated by each algorithm is provided in Supplementary Fig. S3.

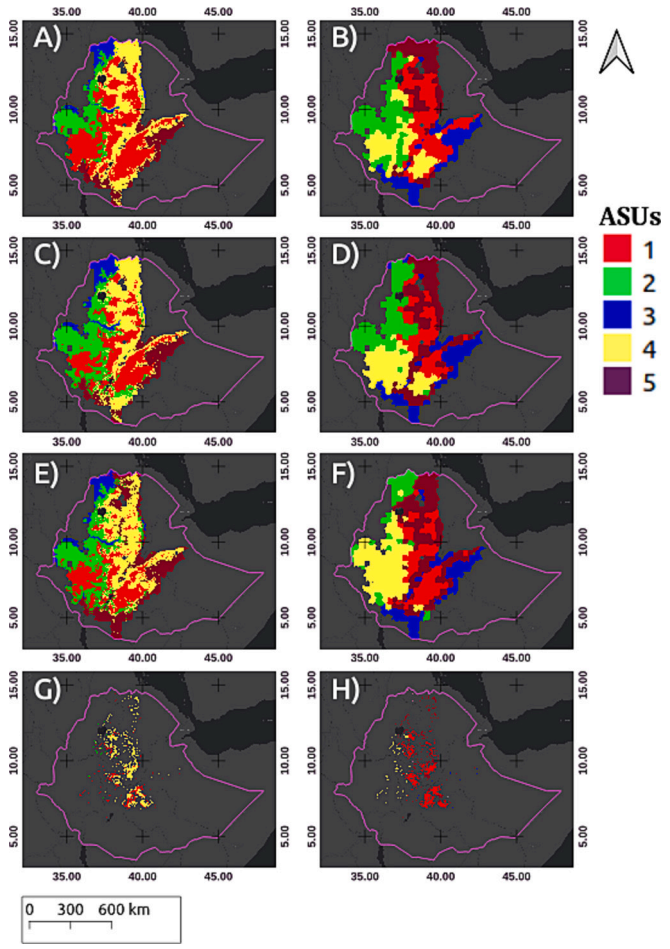

Fig. 3. | Agro-ecological spatial units (ASUs) delineated for Ethiopian rainfed wheat using pixel- and object-based clustering approaches. Panels (A), (C), and (E) depict pixel-based ASUs for the 2021 and 2022 growing seasons, and aggregated ASUs derived from time series data for the period 2016–2022, respectively. Panels (B), (D), and (F) display object-based ASUs for the 2021 and 2022 growing seasons, and aggregated ASUs (2016 to 2022), respectively. Panels (G) and (H) display aggregate ASUs for the rainfed wheat area only (see Fig. 2).

followed by ASU 4 (Fig. 3H and Fig. 4D). The rainfed wheat area represented by ASUs 1, 2, and 3 using the pixel-based approach was about 20 % larger in 2021 than in 2022. This difference in area coverage was less pronounced with the object-based approach, showing variations of up to 10 % of the wheat area between the two growing seasons. Significant discrepancies were noted between the year-specific ASUs and the aggregated ASUs, regardless of the clustering approach, indicating that aggregated ASUs were less effective at capturing year-specific variations. Overall, changes in the wheat area of each ASU were less significant than those within individual ASUs, suggesting that the total spatial coverage of ASUs across the wheat belt remained relatively stable, while their dominance within or outside the rainfed wheat area shifted over time (see Figs. 4A and 4B for the wheat belt and Figs. 4C and 4D for the wheat area). Temporal dynamism was more evident with the pixel-based approach than with the object-based approach across the wheat belt (Figs. 3A-3D; Figs. 4A and B) and the rainfed wheat area within individual ASUs (Figs. 4C and D), underscoring the greater sensitivity of the pixel-based approach to temporal shifts in production environments.

3.3. Evaluation of clustering performance

A Kruskal-Wallis test revealed a significant difference between the pixel-based ASUs (Fig. 5A) and the object-based ASUs (Fig. 5B) for most variables, including NDVI, GDD, pH, elevation, and the aridity index. However, no significant differences were observed for temperature seasonality and PAWC across the object-based ASUs (Fig. 5B). The separability between ASUs in both clustering approaches was further evaluated using wheat yield data from the 2022 growing season, which revealed statistically significant yield differences across ASUs (Supplementary Fig. S6). The clustering quality assessment revealed significant cohesion within ASUs as well as separation among them, as indicated by average silhouette coefficients of 0.51 for pixel-based ASUs and 0.59 for object-based ASUs (Figs. 5C and 5D).

The similarity and complementarity between ASUs developed for different periods with pixel- and object-based approaches is illustrated in Fig. 6. Overall, pixel- and object-based ASUs showed considerable similarity, though some notable dissimilarities were observed as well (Fig. 5A). For instance, object-based ASU 1 displayed high similarity with pixel-based ASUs 1 and 5, while object-based ASU 5 displayed high dissimilarity with pixel-based ASU 5. Other pairwise comparisons of ASUs showed more moderate levels of (dis)similarity.

The similarity matrix also highlighted both stability and dynamism between the single-year 2022 and aggregate ASUs in both clustering approaches (Figs. 6B and 6C). Stability was indicated by higher similarity, while dynamism was reflected by greater dissimilarity between ASUs over different time perspectives. With the pixel-based approach, most aggregate ASUs and single-year ASUs demonstrated a notable degree of stability, except for the slight dynamism observed in ASU 1 (Fig. 6B). Conversely, the object-based approach showed stronger stability in ASU 1 and 5 across the two-time perspectives, while ASU 4 showed stronger dynamism and ASUs 2 and 3 showed slight dynamism. Thus, while substantial stability was observed between aggregated and single-year ASUs with both clustering approaches, certain ASUs - such as ASU 1 in the pixel-based approach and ASU 4 in the object-based approach - exhibited notable instability across the two-time perspectives.

3.4. Characterization of rainfed wheat production environments in Ethiopia

The wheat area maps and the delineated ASUs were used to characterize the Ethiopian wheat cropland based on its agro-ecological characteristics and scope for cropland expansion (Table 1). For instance, pixel-based and object-based ASU 1 was designated as "*prime highlands for rainfed wheat*" due to its significant contribution to rainfed wheat cultivation. Currently, it accounts for 27 % of the total rainfed wheat area with the pixel-based approach and 43 % with the object-based approach, with both located at favorable altitudes for wheat production. Similarly, pixel-based ASU 4 and object-based ASU 5, covering 65 % and 35 % of the total rainfed wheat area, respectively, were designated as "*favorable mid-altitude rainfed wheat environments*". These units cover mid-altitude regions and reflect favorable, albeit more variable, climatic conditions compared to the prime highland. The 'prime' and 'favorable' categories combined constituted approximately 90 % of the total rainfed wheat area and 49 % of the total wheat belt with the pixel-based approach. With the object-based approach, they accounted for 80 % of the rainfed wheat area and 47 % of the wheat belt. Pixel-based ASU 2 and object-based ASU 4, located in the mid-altitude regions with favorable climatic conditions but limited current cultivation, were designated as "*emerging mid-altitude rainfed wheat environments*". These units exhibit significant biophysical potential for rainfed wheat cultivation, covering 21 % and 28 % of the rainfed wheat belt with pixel- and object-based approaches, respectively. Conversely, ASUs situated in low-altitude regions with unfavorable climatic conditions and minimal or no wheat cultivation were categorized as "*low-altitude*

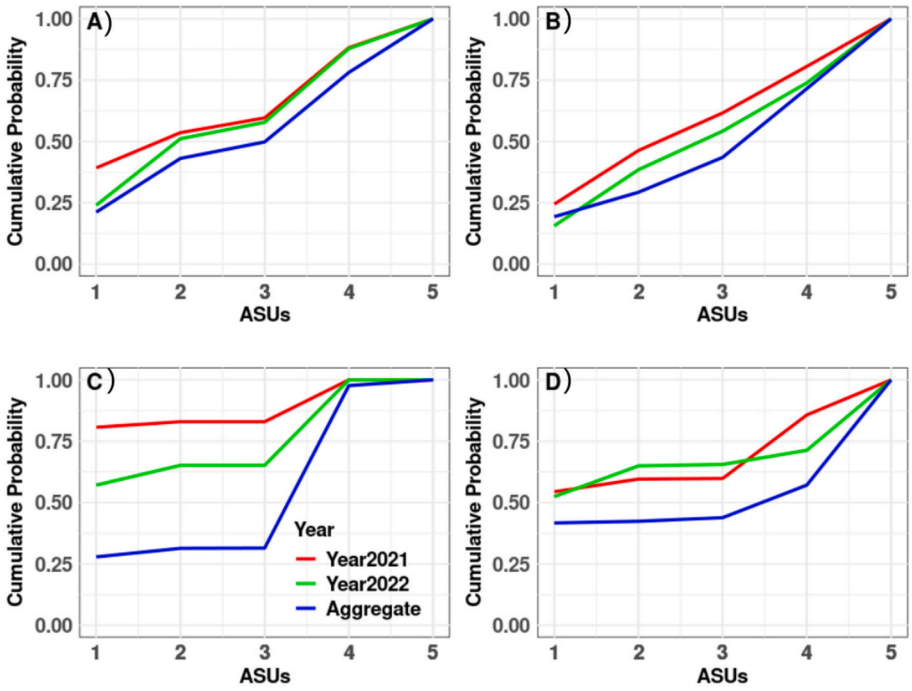

Fig. 4. | Cumulative probability distribution and changes of the area covered by agro-ecological spatial units (ASUs) across the rainfed wheat belt (A, B) and the rainfed wheat area (C, D) using pixel- (A, C) and object-based (B, D) clustering approaches. The rainfed wheat area coverage within each ASU was further used for characterization and logical naming (see Section 3.4).

rainfed wheat frontiers" (e.g., pixel-based ASU 3 and object-based ASU 2) and "*low-altitude rainfed wheat void environments*" (e.g., pixel-based ASU 5 and object-based ASU 3). These represent marginal environments for rainfed wheat production, with the "frontier" category holding limited potential for future cultivation and the "void" category reflecting areas entirely unsuitable for rainfed wheat. However, wheat cultivation in these areas might be possible in the future with available supplemental irrigation.

4. Discussion

We developed a spatial framework by combining rainfed wheat area mapping (Section 4.1) with the delineation of dynamic ASUs (Section 4.2) to characterize Ethiopia's rainfed wheat production environments. This framework offers a holistic perspective by linking biophysical production potential with actual cultivation, enabling the analysis of current coverage and future cropland expansion (Section 4.3). Beyond its application to Ethiopia's complex landscape, the framework demonstrates broader agronomic relevance and can be adapted for other regions and crops (Section 4.4).

4.1. Insights from rainfed wheat area mapping in Ethiopia

In this study, we employed an ensemble machine learning approach based on ground truth observations, remote sensing, and biophysical variables to map the annual rainfed wheat area distribution in Ethiopia for two growing seasons. Rainfed wheat area mapping across two growing seasons revealed an expansion of 0.26 Mha from 2021 to 2022, highlighting the evolving pattern of rainfed wheat cultivation in Ethiopia and its alignment with official statistics on cropland expansion trends (CSA, 2022; FAOSTAT, 2022). Results also highlight the large share of rainfed wheat areas in the Oromia and Amhara regions. Together, these regions contributed more than 91 % of the estimated national rainfed wheat area (Fig. 5), being of strategic importance to the country's wheat sector growth and its broader agricultural development.

The proposed approach achieved an overall modeling accuracy of 88 % for the 2021 growing season and 94 % for the 2022 growing season. The higher accuracy observed in this study compared to earlier studies (Eisfelder et al., 2024; Khatami et al., 2020; Delrue et al., 2013) can be attributed to three key methodological enhancements. First, the use of multi-source high-resolution data - the integration of Sentinel-1 and Sentinel-2, coupled with derived vegetation indices as well as seasonal and crop phenological information - enabled more precise discrimination between wheat and other crops (Inglada et al., 2016; Ofori-Ampofo et al., 2021; Orynbaikyzy et al., 2019; Orynbaikyzy et al., 2020; Al-Shammari et al., 2020; Ashourloo et al., 2022; Felegari et al., 2021). Second, incorporating biophysical variables, such as elevation and climate, significantly improved mapping accuracy. Elevation, for instance, influences microclimates and soil properties, determining the suitability and spatial distribution of wheat (Alemayehu et al., 2024). Third, the ensemble approach leveraged the complementary strengths of individual models rather than relying on a single model, improving classification accuracy, a finding consistent with recent studies (Walhazi et al., 2024; Ahmed et al., 2023; Mahajan et al., 2023; Sagi and Rokach, 2018; Pourdarbani et al., 2019). The proposed method offers significant advantages over generic crop distribution datasets that do not account for specific crop growing seasons (e.g., You and Guo, 2024). By providing crop-specific area estimates, our approach effectively captures both spatial and temporal patterns of land cultivation under smallholder farming conditions.

4.2. Dynamic agro-ecological spatial units: a scalable framework for evolving production environments

The dynamic agro-ecological spatial units (ASUs) developed in this study offer a robust and scalable framework for characterizing production environments. Our approach balanced the trade-off between oversimplification and excessive fragmentation by delineating ASUs specific to rainfed wheat, clustering production environments based on shared characteristics, (Supplementary Fig. S3), and determining the optimal number of ASUs through quantitative validation (Supplementary

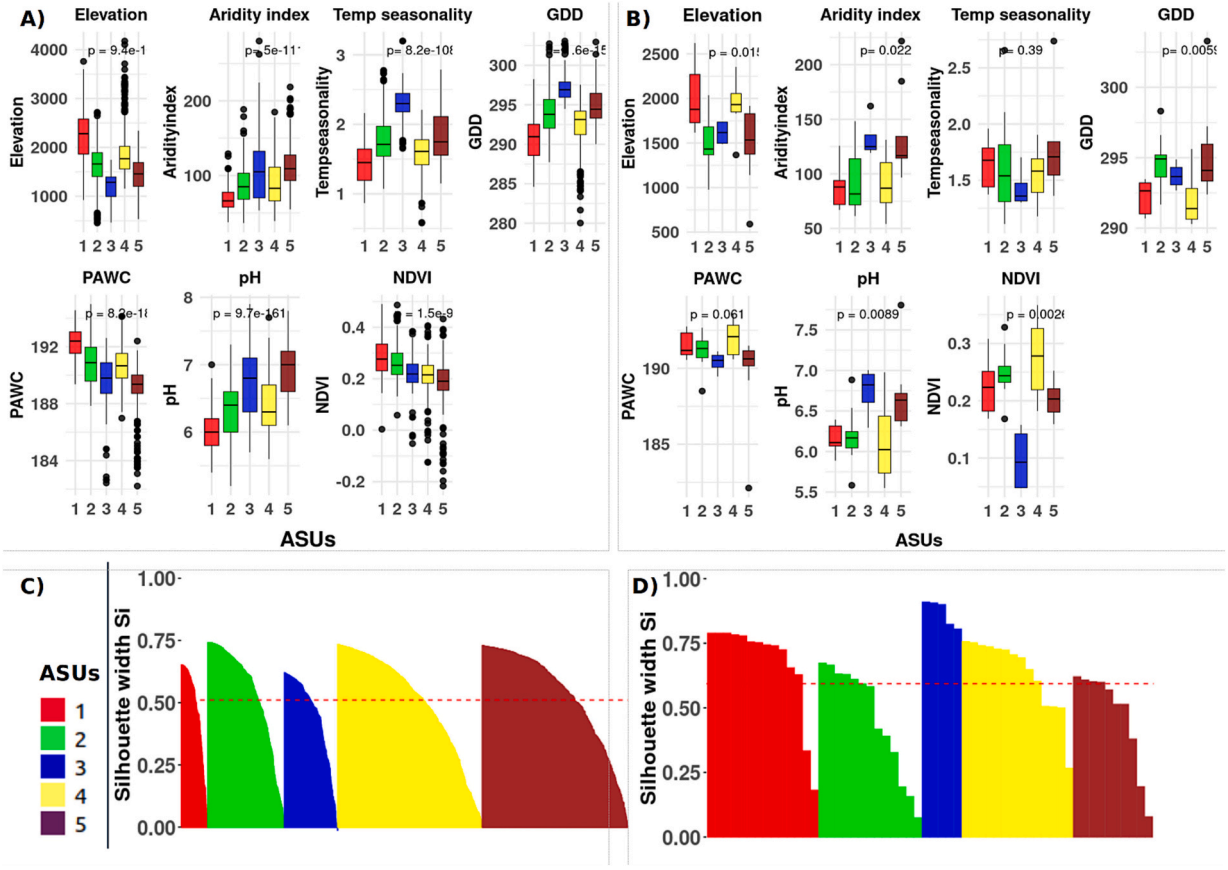

Fig. 5. | Internal clustering evaluation illustrates the variability between agro-ecological spatial units (ASUs) and clustering quality for both pixel- and object-based approaches. Panels (A) and (B) display the Kruskal-Wallis test showing the statistical differences between ASUs for pixel- and object-based ASUs, respectively. This test is accompanied by boxplots that illustrate the distribution of selected variables across ASUs and are used in the characterization and naming of the ASUs (see Section 3.4 for further details). Panels (C) and (D) display the clustering quality using the silhouette coefficient for both pixel- and object-based approaches, respectively. Each bar in (C) and (D) refers to one grid cell (Fig. 4) and dashed red lines display the mean silhouette coefficient for each clustering approach.

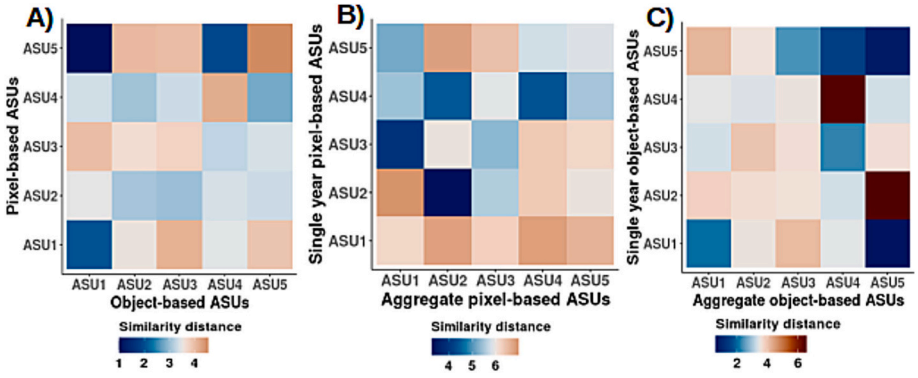

Fig. 6. | Similarity and temporal scalability assessment of agro-ecological spatial units (ASUs) produced with different approaches: (A) similarity between aggregate object- and pixel-based ASUs, (B) temporal scalability and dynamism for pixel-based ASUs, and (C) temporal scalability and dynamism for object-based ASUs. Temporal scalability and dynamism considered the ASUs from the 2022 growing season and the aggregate ASUs. A log transformation was applied to the original distance matrix to improve readability. A darker shade of blue denotes a stronger similarity between ASUs developed with different approaches, while dark red denotes the opposite.

Fig. S4). This process revealed spatial patterns that informed the clustering analysis, resulting in maximum homogeneity within ASUs while minimizing the number of ASUs needed to represent the Ethiopian rainfed wheat belt. This framework offered distinct advantages over previous studies relying on matrix zonation based on expert knowledge (e.g., Edreira et al., 2018; van Wart et al., 2013; Mueller et al., 2012), which were limited by categorical variables that failed to capture the structure of the input data. Both pixel- and object-based ASUs exhibited similar characteristics (Fig. 6A) and spatial arrangement (Fig. 4A-4F), with consistency between single-year and aggregate ASUs (Figs. 6B and 6C). Internal and external evaluation metrics demonstrated the reliability of the framework to segment crop production environments.

Combining pixel- and object-based approaches ensured spatial scalability, making the framework adaptable for characterizing crop

Table 1
| Characterization and logical naming of agro-ecological spatial units (ASUs) for rainfed wheat production environments based on key biophysical variables (Fig. 5A and B), rainfed wheat area coverage (Figs. 4C and 4D, Figs. 3G and 3H), and pairwise similarity matrix- based variable associations with elevation serving as a linking factor for clustering due to its strong correlation with other variables (Supplementary Fig. S4). Logical names were assigned to each ASU to reflect its potential for rainfed wheat production.

Pixel-based ASUs	Object-based ASUs	Key features			Rainfed wheat area coverage	Logical name
		Altitude	Climate condition	Soil condition		
ASU 1	ASU 1					Prime highlands for rainfed wheat
ASU 4	ASU 5					Favorable mid-altitude regions for rainfed wheat
ASU 2	ASU 4					Emerging mid-altitude regions for rainfed wheat
ASU 3	ASU 2					Low-altitude rainfed wheat frontier
ASU 5	ASU 3					Low-altitude rainfed wheat void

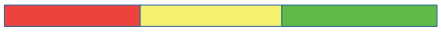

production environments across spatial scales. Pixel-based ASUs unveiled spatial patterns at high resolution (Fig. 4A-C), making them suitable for agronomic assessments at the local level (e.g., Stuart et al., 2016). In contrast, object-based ASUs produced coarser yet more interpretable ASUs (Fig. 4D-F), enabling their application for agronomic assessments at a national level. This flexibility addresses the challenge of creating spatial frameworks that balance the aggregation benefits of object-based ASUs with the detailed climate and soil variability captured by the pixel-based ASUs. As highlighted by van Wart et al. (2013) and Rattalino Edreira et al. (2018), this scalability ensures the framework can be tailored to the spatial scale of interest. Pixel-based ASUs 3, 4, and 5 differed from their object-based counterparts, highlighting the complementary nature of these approaches (Fig. 6A). This complementarity helps in the characterization of diverse crop production environments.

The delineated ASUs with both pixel- and object-based approaches were temporally scalable yet dynamic, providing valuable agronomic insights. Furthermore, the consistent agreement between year-specific ASUs and aggregate ASUs underscores the framework's capacity to operate effectively across different periods. It revealed the framework's ability to capture both short-term fluctuations - such as growing season-specific weather conditions - and longer-term patterns resulting from changing climatic conditions. Such versatility positions the framework as a valuable tool for informing climate change adaptation strategies for wheat in Ethiopia, as emphasized by Alemayehu et al. (2024). The framework also remains dynamic, as evidenced by observed changes in specific ASUs (Fig. 6), reflecting the framework's ability to capture evolving changes in production environments.

4.3. Integrating rainfed wheat area with agro-ecological spatial units to characterize production environments

Integrating crop area mapping with dynamic ASUs delineation enabled the identification of ASUs where rainfed wheat cultivation is viable and where it remains constrained (Figs. 3G and 3H). ASUs exhibited varying levels of potential for rainfed wheat cultivation (Table 1), ranging from units with favorable biophysical conditions, encompassing large portions of the rainfed wheat area, to those with minimal potential due to environmental constraints.

The prime and favorable units, predominantly situated in high- and mid-altitude regions, represent 90 % of Ethiopia's rainfed wheat area with the pixel-based approach and 80 % with the object-based clustering. These findings align with earlier studies (Simane et al., 1999; Semahegn et al., 2021; Alemayehu et al., 2024), which identified mid- and high-altitude regions (1500–3000 m) as ideal for rainfed wheat due to reliable precipitation, favorable temperatures, and fertile soils.

Mid-altitude ASUs characterized by favorable climatic conditions but limited current rainfed wheat cultivation, encompassing regions with potential for future rainfed wheat cultivation, despite their currently limited cultivation. These limitations are likely linked to socio-economic factors, rather than environmental unsuitability (Semahegn et al., 2021). Improved infrastructure, extension services, and adoption of modern agricultural practices could unlock the potential of these units and further increase wheat cropland in Ethiopia.

Low-altitude ASUs, where rainfed wheat cultivation is limited or absent, are less viable for rainfed wheat production due to unfavorable climatic conditions compounded with low soil fertility (Simane et al., 1999; Hailu et al., 2015; Girmay et al., 2018; Nahusenay and Kibebew, 2015). Yet, they could hold a promise for future wheat production with appropriate interventions and adaptive strategies, such as the introduction of drought-tolerant wheat varieties (White et al., 2001), the implementation of soil and water conservation measures, and investments in irrigation schemes (Girmay et al., 2018; and Hailu et al., 2015).

4.4. Agronomic relevance and transferability

ASUs can play a pivotal role in the contextualization of agronomic analysis by considering agroecological factors such as soil type, climate, and topography, providing a detailed understanding of local conditions. When integrated with socioeconomic data, the framework can tailor agricultural technologies to specific contexts (Araya et al., 2010; Muthoni et al., 2017; Tesfaye et al., 2015). For instance, it can guide fertilizer advisories (Liben et al., 2024), ensuring that recommendations address the unique challenges and constraints of each ASU. This localized approach can further enhance the adoption of agronomic technologies and promote sustainable agriculture (Muthoni et al., 2017).

Furthermore, the framework can facilitate the scaling out of local agronomic technologies and findings to larger geographic areas with similar biophysical characteristics (Grassini et al., 2017; Rattalino Edreira et al., 2018). Additionally, ASUs can optimize resource allocation by identifying areas where resources are overused or underused and matching agricultural technologies to the capabilities and limitations of each spatial unit, as demonstrated by Klein et al. (2013). Lastly, the framework could support the ex-ante evaluation of agricultural technologies across spatial scales, from local to regional levels (Andrade et al., 2019).

The framework can be adaptable and transferable to other crops and production environments in a cost-effective way. For instance, feature engineering will require crop-specific adjustments tailored to the site-specific context. This will be especially important for remote sensing-derived features, such as seasonal parameters and vegetation indices, as well as environmental data, which are crop and growing season-dependent (Supplementary Table 1). Including time series information for time-variant features will remain important to ensure temporal transferability and capture inter- and intra-annual variations in the crop production environment. From a methodological standpoint, pre-cluster data exploration and defining the optimum number of clusters in a data-driven manner are necessary to balance oversimplification and hyper-segmentation of production environments. Dynamic clustering algorithms can further enhance this process (Zhang and Hepner, 2017). Lastly, we recommend assembling data stacks with ground truth observations on crop type presence and measured crop yields for accurate crop type maps and evaluating the performance of the clustering analysis in data-rich environments. For data-poor regions, internal evaluation techniques based on dissimilarity analysis across the feature space should be preferred (Hardy Kremer et al., 2011; Brun et al., 2007).

5. Conclusions

We developed a data-driven framework to delineate crop-specific and time-variant agro-ecological spatial units (ASUs) for characterizing crop production environments. The framework involved mapping rainfed wheat areas in Ethiopia during the 2021 and 2022 growing seasons with an ensemble machine-learning approach. The ensemble model demonstrated high predictive accuracy (>90 %) and strong generalizability across the two growing seasons. The framework also delineated crop-specific time-variant ASUs through pixel- and object-based clustering algorithms. The spatial-temporally scalable and dynamic ASUs were specifically developed for Ethiopia's rainfed wheat belt. Their spatial scalability enables the characterization of production environments at various spatial scales, while their temporal dynamism facilitates the analysis of both short-term fluctuations and longer-term changes in crop production environments. This spatial and temporal flexibility ensures the framework's ability to capture changes in crop production environments across space and time, making it a valuable tool to support food security and environmental assessments.

CRediT authorship contribution statement

Habtamu S. Gelagay: Writing – review & editing, Writing – original draft, Visualization, Validation, Software, Methodology, Investigation, Formal analysis, Data curation, Conceptualization. **Louise Leroux:** Writing – review & editing, Writing – original draft, Validation, Supervision, Resources, Project administration, Methodology, Investigation, Funding acquisition, Conceptualization. **Lulseged Tamene:** Writing – review & editing, Supervision, Resources. **Meklit Chernet:** Writing – review & editing, Conceptualization. **Gerald Blasch:** Writing – review & editing, Data curation. **Degefie Tibebe:** Writing – review & editing, Data curation. **Wuletawu Abera:** Writing – review & editing, Conceptualization. **Tesfaye Sida:** Writing – review & editing, Data curation. **Kindie Tesfaye:** Writing – review & editing, Data curation. **Marc Corbeels:** Writing – review & editing, Validation, Supervision, Resources, Project administration, Funding acquisition, Conceptualization. **João Vasco Silva:** Writing – review & editing, Writing – original draft, Methodology, Conceptualization.

Declaration of competing interest

We declare that there are no conflicts of interest associated with this manuscript. All authors have reviewed the final version of the manuscript and approve it for submission.

Acknowledgments

This study was funded by the OneCGIAR Research Excellence in Agronomy Initiative (INV-005431). Habtamu Gelagay received a fellowship from the French Space Agency (CNES) and was supported by the French National Research Agency under the Investments for the Future Program (ANR-16-CONV-0004). The authors wish to thank CIAT-Ethiopia and CIMMYT-Ethiopia for providing the ground-truth observations used in this study.

Appendix A. Supplementary data

Supplementary data to this article can be found online at https://doi.org/10.1016/j.agsy.2025.104360.

Data availability

All the geospatial data used are freely available under Google Earth Engine (https://developers.google.com/earth-engine/datasets/catalog). Data produced by this study (wheat crop area and ASUs maps) will be made available upon request.

References

Abatzoglou, J.T., Dobrowski, S.Z., Parks, S.A., Hegewisch, K.C., 2018. TerraClimate, a high-resolution global dataset of monthly climate and climatic water balance from 1958–2015. Sci. Data 5 (1), 1–12.

Ahmed, S., Mahmoud, A.S., Farg, E., Mohamed, A.M., Moustafa, M.S., Abutaleb, K., Saleh, A.M., AbdelRahman, M.A.E., AbdelSalam, H.M., Arafat, S.M., 2023. Investigation on the use of ensemble learning and big data in crop identification. Heliyon 9 (2), e13339. https://doi.org/10.1016/j.heliyon.2023.e13339.

Alemayehu, S., Olago, D., Opere, A., Zeleke, T.T., Dejene, S.W., 2024. Evaluating wheat cultivation potential in Ethiopia under the current and future climate change scenarios. Land 13 (11), 1915.

Al-Shammari, D., Fuentes, I., Whelan, M., Filippi, P., FA Bishop, T., 2020. Mapping of cotton fields within season using phenology-based metrics derived from a time series of Landsat imagery. Remote Sens. 12 (18), 3038.

Amede, T., Gashaw, T., Legesse, G., Tamene, L., Mekonen, K., Thorne, P., Schultz, S., 2022. Landscape positions dictating crop fertilizer responses in wheat-based farming systems of east African highlands. Renew. Agric. Food Syst. 37 (S1), S4–S16. https://doi.org/10.1017/S1742170519000504.

Andrade, J.F., Edreira, J.I.R., Farrow, A., van Loon, M.P., Craufurd, P.Q., Rurinda, J., Grassini, P., 2019. A spatial framework for ex-ante impact assessment of agricultural technologies. Glob. Food Sec. 20, 72–81.

Araya, A., Keesstra, S.D., Stroosnijder, L., 2010. A new agro-climatic classification for crop suitability zoning in northern semi-arid Ethiopia. Agric. For. Meteorol. 150 (7–8), 1057–1064.

Arthur, D., & Vassilvitskii, S. (2007). K-means++: the advantages of careful seeding. In soda (Vol. 7, pp. 1027-1035).

Ashourloo, D., Nematollahi, H., Huete, A., Aghighi, H., Azadbakht, M., Shahrabi, H.S., Goodarzdashti, S., 2022. A new phenology-based method for mapping wheat and barley using a time series of Sentinel-2 images. Remote Sens. Environ. 280, 113206. https://doi.org/10.1016/j.rse.2022.113206.

Beckham, C., Hall, M., Frank, E., 2016. WekaPyScript: classification, regression, and filter schemes for WEKA implemented in python. J. Open Res. Softw. 4 (1) e33-e33.

Bellón, B., Bégué, A., Lo Seen, D., De Almeida, C.A., Simões, M., 2017. A remote sensing approach for regional-scale mapping of agricultural land-use systems based on NDVI time series. Remote Sens. 9 (6), 600.

Beza, E., Silva, J.V., Kooistra, L., Reidsma, P., 2017. Review of yield gap explaining factors and opportunities for alternative data collection approaches. Eur. J. Agron. 82, 206–222. https://doi.org/10.1016/j.eja.2016.06.016.

Bittencourt, J.C.N., Costa, D.G., Portugal, P., Vasques, F., 2024. A data-driven clustering approach for assessing spatiotemporal vulnerability to urban emergencies. Sustain. Cities Soc. 108, 105477.

Bokonda, P.L., Ouazzani-Touhami, K., Souissi, N., 2020. Predictive analysis using machine learning: Review of trends and methods. In: 2020 International Symposium on Advanced Electrical and Communication Technologies (ISAECT). IEEE, pp. 1–6.
Breiman, L., 2001. Random forests. Mach. Learn. 45 (1), 5–32. https://doi.org/10.1023/A:1010933404324.
Breimann, L., Friedman, J.H., Olshen, R.A., Stone, C.J., 1984. Classification and Regression Trees, Pacific Grove. Wadsworth.
Brun, M., Sima, C., Hua, J., Lowey, J., Carroll, B., Suh, E., Dougherty, E.R., 2007. Model-based evaluation of clustering validation measures. Pattern Recogn. 40 (3), 807–824. https://doi.org/10.1016/j.patcog.2006.06.026.
Cao, F., Liang, J., Li, D., Bai, L., Dang, C., 2012. A dissimilarity measure for the k-modes clustering algorithm. Knowl.-Based Syst. 26, 120–127. https://doi.org/10.1016/j.knosys.2011.07.011.
Cassman, K.G., Grassini, P., 2020. A global perspective on sustainable intensification research. Nat. Sustain. 3 (4), 262–268.
Central Statistical Agency, 2021. The Federal Democratic Republic of Ethiopia Central Statistical Agency, Agricultural Sample Survey (2013 E.C.), Volume I, Report on Area and Production of Major Crops (Private Peasant Holdings, Meher Season) Statistical Bulletin 590. Addis Ababa, Ethiopia.
Central Statistics Agency (CSA). 2022a. Agriculture sample survey 2021/2022 (2014 E.C.). Statistical bulletin, report on report on area and production of major crops (private peasant holdings, Meher season). Addis Ababa: CSA. http://www.statsethiopia.gov.et/wp-content/uploads/2023/05/The-2014-EC-Meher-Season-Report-on-Area-and-Production-of-Major-Crops_Final-1.pdf.
Congalton, R.G., Green, K., 2019. Assessing the Accuracy of Remotely Sensed Data: Principles and Practices. CRC Press.
Delrue, J., Bydekerke, L., Eerens, H., Gilliams, S., Piccard, I., Swinnen, E., 2013. Crop mapping in countries with small-scale farming: a case study for west Shewa, Ethiopia. Int. J. Remote Sens. 34 (7), 2566–2582. https://www.tandfonline.com/doi/abs/10.1080/01431161.2012.747016.
Di Falco, S., Chavas, J.P., Smale, M., 2007. Farmer management of production risk on degraded lands: the role of wheat variety diversity in the Tigray region, Ethiopia. Agric. Econ. 36 (2), 147–156.
Edreira, J.I.R., Cassman, K.G., Hochman, Z., Van Ittersum, M.K., Van Bussel, L., Claessens, L., Grassini, P., 2018. Beyond the plot: technology extrapolation domains for scaling out agronomic science. Environ. Res. Lett. 13 (5), 054027.
Eisfelder, C., Boemke, B., Gessner, U., Sogno, P., Alemu, G., Hailu, R., Mesmer, C., Huth, J., 2024. Cropland and crop type classification with Sentinel-1 and Sentinel-2 time series using Google earth engine for agricultural monitoring in Ethiopia. Remote Sens. 16 (5), 5. https://doi.org/10.3390/rs16050866.
Farr, T.G., Rosen, P.A., Caro, E., Crippen, R., Duren, R., Hensley, S., Alsdorf, D., 2007. The shuttle radar topography mission. Rev. Geophys. 45 (2).
Felegari, S., Sharifi, A., Moravej, K., Amin, M., Golchin, A., Muzirafuti, A., Tariq, A., Zhao, N., 2021. Integration of sentinel 1 and sentinel 2 satellite images for crop mapping. Appl. Sci. 11 (21), 21. https://doi.org/10.3390/app112110104.
Food and Agriculture Organization of the United Nations, 2022. FAOSTAT: Crop and livestock database. Retrieved January 25, 2024, from. https://www.fao.org/faostat/en/#data/QCL.
Fraley, C., Raftery, A.E., 1998. How many clusters? Which clustering method? Answers via model-based cluster analysis. Comput. J. 41 (8), 578–588.
Friedman, J.H., 2001. Greedy function approximation: a gradient boosting machine. Ann. Stat. 1189–1232.
Fritz, S., See, L., McCallum, I., You, L., Bun, A., Moltchanova, E., Duerauer, M., Albrecht, F., Schill, C., Perger, C., Havlik, P., Mosnier, A., Thornton, P., Wood-Sichra, U., Herrero, M., Becker-Reshef, I., Justice, C., Hansen, M., Gong, P., Obersteiner, M., 2015. Mapping global cropland and field size. Glob. Chang. Biol. 21 (5), 1980–1992. https://doi.org/10.1111/gcb.12838.
Funk, C., Peterson, P., Landsfeld, M., Pedreros, D., Verdin, J., Shukla, S., Michaelsen, J., 2015. The climate hazards infrared precipitation with stations—a new environmental record for monitoring extremes. Sci. Data 2 (1), 1–21.
Gao, X., 2010. Composite likelihood Bayesian information criteria for model selection in high-dimensional data. J. Am. Stat. 105 (492), 1531–1540.
Ghazaryan, G., Dubovyk, O., Löw, F., Lavreniuk, M., Kolotii, A., Schellberg, J., Kussul, N., 2018. A rule-based approach for crop identification using multi-temporal and multi-sensor phenological metrics. Eur. J. Remote Sensing 51 (1), 511–524. https://doi.org/10.1080/22797254.2018.1455540.
Giller, K.E., Delaune, T., Silva, J.V., van Wijk, M., Hammond, J., Descheemaeker, K., Andersson, J.A., 2021. Small farms and development in sub-Saharan Africa: Farming for food, for income or for lack of better options? Food Secur. 13 (6), 1431–1454.
Girmay, G., Sebnie, W., Reda, Y., 2018. Land capability classification and suitability assessment for selected crops in Gateno watershed, Ethiopia. Cogent Food & Agric. 4 (1), 1532863.
Gorelick, N., Hancher, M., Dixon, M., Ilyushchenko, S., Thau, D., Moore, R., 2017. Google earth engine: planetary-scale geospatial analysis for everyone. Remote Sens. Environ. 202, 18–27. https://doi.org/10.1016/j.rse.2017.06.031.
Grassini, P., Pittelkow, C.M., Cassman, K.G., Yang, H.S., Archontoulis, S., Licht, M., Guindin-Garcia, N., 2017. Robust spatial frameworks for leveraging research on sustainable crop intensification. Glob. Food Sec. 14, 18–22.
Green, P.E., Rao, V.R., 1969. A Note on Proximity Measures and Cluster Analysis.
Grossman, R.B., Reinsch, T.G., 2002. 2.1 Bulk Density and Linear Extensibility. In: Methods of Soil Analysis: Part 4 Physical Methods, 5, pp. 201–228.
Hailu, A.H., Kibret, K., Gebrekidan, H., 2015. Land suitability evaluation for rainfed production of barley and wheat at Kabe subwatershed, Northeastern Ethiopia. Afr. J. Soil Sci. 3 (7), 147–156.
Hardy Kremer, Philipp Kranen, Timm Jansen, Seidl, Thomas, Bifet, Albert, Geoff Holmes, 2011. An effective evaluation measure for clustering on evolving data streams. In: ACM SIGKDD, pp. 868–876.
Headey, D., Dereje, M., Taffesse, A.S., 2014. Land constraints and agricultural intensification in Ethiopia: a village-level analysis of high-potential areas. Food Policy 48, 129–141. https://doi.org/10.1016/j.foodpol.2014.01.008.
Hengl, T., Miller, M.A., Križan, J., Shepherd, K.D., Sila, A., Kilibarda, M., Crouch, J., 2021. African soil properties and nutrients mapped at 30 m spatial resolution using two-scale ensemble machine learning. Sci. Rep. 11 (1), 6130.
Inglada, J., Vincent, A., Arias, M., Marais-Sicre, C., 2016. Improved early crop type identification by joint use of high temporal resolution SAR and optical image time series. Remote Sens. 8 (5), 5. https://doi.org/10.3390/rs8050362.
Jakubauskas, M.E., Legates, D.R., Kastens, J.H., 2001. Harmonic analysis of time-series AVHRR NDVI data. Photogramm. Eng. Remote. Sens. 67 (4), 461–470.
Jakubauskas, M.E., Legates, D.R., Kastens, J.H., 2002. Crop identification using harmonic analysis of time-series AVHRR NDVI data. Comput. Electron. Agric. 37 (1), 127–139. https://doi.org/10.1016/S0168-1699(02)00116-3.
Jonsson, P., Eklundh, L., 2002. Seasonality extraction by function fitting to a time series of satellite sensor data. IEEE Trans. Geosci. Remote Sens. 40 (8), 1824–1832. https://doi.org/10.1109/TGRS.2002.802519.
Kassawmar, T., Eckert, S., Hurni, K., Zeleke, G., Hurni, H., 2018. Reducing landscape heterogeneity for improved land use and land cover (LULC) classification across the large and complex Ethiopian highlands. Geocarto Int. 33 (1), 53–69.
Kaufman, L., Rousseeuw, P.J., 2009. Finding Groups in Data: An Introduction to Cluster Analysis, New York, vol. 344. John Wiley & Sons. ISBN: 0–471–87876-6 Google Scholar.
Khatami, R., Southworth, J., Muir, C., Caughlin, T., Ayana, A.N., Brown, D.G., Agrawal, A., 2020. Operational large-area land-cover mapping: an Ethiopia case study. Remote Sens. 12 (6), 954.
Klaus, V.H., Boch, S., Boeddinghaus, R.S., Hölzel, N., Kandeler, E., Marhan, S., Kleinebecker, T., 2016. Temporal and small-scale spatial variation in grassland productivity, biomass quality, and nutrient limitation. Plant Ecol. 217, 843–856.
Klein, T., Holzkämper, A., Calanca, P., Seppelt, R., Fuhrer, J., 2013. Adapting agricultural land management to climate change: a regional multi-objective optimization approach. Landsc. Ecol. 28, 2029–2047.
Koldasbayeva, D., Tregubova, P., Gasanov, M., Zaytsev, A., Petrovskaia, A., Burnaev, E., 2024. Challenges in data-driven geospatial modeling for environmental research and practice. Nat. Commun. 15 (1), 10700.
Kruskal, W.H., Wallis, W.A., 1952. Use of ranks in one-criterion variance analysis. J. Am. Stat. Assoc. 47 (260), 583–621.
Kwedlo, W., 2011. A clustering method combining differential evolution with the *K*-means algorithm. Pattern Recogn. Lett. 32 (12), 1613–1621. https://doi.org/10.1016/j.patrec.2011.05.010.
Liang, J., Chen, C., Song, Y., Sun, W., Yang, G., 2023. Long-term mapping of land use and cover changes using Landsat images on the Google earth engine cloud platform in the bay area, a case study of Hangzhou Bay, China. Sustain. Horiz. 7, 100061.
Liben, F., Abera, W., Chernet, M.T., Ebrahim, M., Tilaye, A., Erkossa, T., Tamene, L., 2024. Site-specific fertilizer recommendations using data-driven machine learning enhanced wheat productivity and resource use efficiency. Field Crop Res. 313, 109413.
Liu, X., Zhai, H., Shen, Y., Lou, B., Jiang, C., Li, T., Hussain, S.B., Shen, G., 2020. Large-scale crop mapping from multisource remote sensing images in Google earth engine. IEEE J. Selec. Top. Appl. Earth Observ. Remote Sens. 13, 414–427. https://doi.org/10.1109/JSTARS.2019.296353.
Mahajan, P., Uddin, S., Hajati, F., Moni, M.A., 2023. Ensemble learning for disease prediction: a review. Healthcare 11 (12), 12. https://doi.org/10.3390/healthcare11121808.
Mersha, E., 2000. Agroclimatic classification of Ethiopia. Ethiopian J. Nat. Resour.
Mi, L., Chen, Z., 2020. Superpixel-enhanced deep neural forest for remote sensing image semantic segmentation. ISPRS J. Photogramm. Remote Sens. 159, 140–152.
Mueller, N.D., Gerber, J.S., Johnston, M., Ray, D.K., Ramankutty, N., Foley, J.A., 2012. Closing yield gaps through nutrient and water management. Nature 490 (7419), 254–257. https://doi.org/10.1038/nature11420.
Muñoz Sabater, J., (2019): ERA5-Land Monthly Averaged Data From 1981 to the Present. Copernicus Climate Change Service (C3S) Climate Data Store (CDS). Doi:10.24381/cds.68d2bb30.
Muthoni, F.K., Guo, Z., Bekunda, M., Sseguya, H., Kizito, F., Baijukya, F., Hoeschle-Zeledon, I., 2017. Sustainable recommendation domains for scaling agricultural technologies in Tanzania. Land Use Policy 66, 34–48. https://doi.org/10.1016/j.landusepol.2017.04.028.
Nahusenay, A., Kibebew, K., 2015. Land suitability evaluation in Wadla Delanta massif of north central highlands of Ethiopia for rainfed crop production. Afr. J. Agric. Res. 10 (13), 1595–1611.
Ndao, B., Leroux, L., Gaetano, R., Diouf, A.A., Soti, V., Bégué, A., Sambou, B., 2021. Landscape heterogeneity analysis using geospatial techniques and a priori knowledge in Sahelian agroforestry systems of Senegal. Ecol. Indic. 125, 107481.
Neath, A.A., Cavanaugh, J.E., 2012. The Bayesian information criterion: background, derivation, and applications. Wiley Interdisc. Rev. Comput. Stat. 4 (2), 199–203.
Ofori-Ampofo, S., Pelletier, C., Lang, S., 2021. Crop type mapping from optical and radar time series using attention-based deep learning. Remote Sens. 13 (22), 4668. https://doi.org/10.3390/rs13224668.
Orynbaikyzy, A., Gessner, U., Conrad, C., 2019. Crop type classification using a combination of optical and radar remote sensing data: a review. Int. J. Remote Sens. 40 (17), 6553–6595. https://doi.org/10.1080/01431161.2019.1569791.
Orynbaikyzy, A., Gessner, U., Mack, B., Conrad, C., 2020. Crop type classification using fusion of Sentinel-1 and Sentinel-2 data: assessing the impact of feature selection,

optical data availability, and parcel sizes on the accuracies. Remote Sens. 12 (17), 17. https://doi.org/10.3390/rs12172779.
Pelleg, D., Moore, A.W., 2000, June. X-means: extending k-means with efficient estimation of the number of clusters. In: ICML, Vol. 1, pp. 727–734.
Porter, J.R., Semenov, M.A., 2005. Crop responses to climatic variation. Philos. Trans. R. Soc. B 360 (1463), 2021–2035. https://doi.org/10.1098/rstb.2005.1752.
Pourdarbani, R., Sabzi, S., Hernández-Hernández, M., Hernández-Hernández, J.L., García-Mateos, G., Kalantari, D., Molina-Martínez, J.M., 2019. Comparison of different classifiers and the majority voting rule for the detection of plum fruits in garden conditions. Remote Sens. 11 (21), 21. https://doi.org/10.3390/rs11212546.
Puzicha, J., Hofmann, T., Buhmann, J.M., 2000. A theory of proximity-based clustering: structure detection by optimization. Pattern Recogn. 33 (4), 617–634. https://doi.org/10.1016/S0031-3203(99)00076-X.
Ramirez-Villegas, J., Challinor, A., 2012. Assessing relevant climate data for agricultural applications. Agric. For. Meteorol. 161, 26–45. https://doi.org/10.1016/j.agrformet.2012.03.015.
Rousseeuw, P.J., 1987. Silhouettes: a graphical aid to the interpretation and validation of cluster analysis. J. Comput. Appl. Math. 20, 53–65. https://doi.org/10.1016/0377-0427(87)90125-7.
Sagi, O., Rokach, L., 2018. Ensemble learning: a survey. Wiley Interdisc. Rev. Data Mining Knowl. Discov. 8 (4), e1249.
See, L., Fritz, S., You, L., Ramankutty, N., Herrero, M., Justice, C., Becker-Reshef, I., Thornton, P., Erb, K., Gong, P., Tang, H., van der Velde, M., Ericksen, P., McCallum, I., Kraxner, F., Obersteiner, M., 2015. Improved global cropland data as an essential ingredient for food security. Glob. Food Sec. 4, 37–45.
Semahegn, Y., Shimelis, H., Laing, M., Mathew, I., 2021. Farmers' preferred traits and perceived production constraints of bread wheat under drought-prone agroecologies of Ethiopia. Agric. Food Secur. 10 (1), 18.
Senbeta, A.F., Worku, W., 2023. Ethiopia's wheat production pathways to self-sufficiency through land area expansion, irrigation advance, and yield gap closure. Heliyon 9 (10). https://doi.org/10.1016/j.heliyon.2023.e20720.
Silva, J.V., Reidsma, P., Baudron, F., Jaleta, M., Tesfaye, K., van Ittersum, M.K., 2021. Wheat yield gaps across smallholder farming systems in Ethiopia. Agron. Sustain. Dev. 41 (1), 12.
Silva, J.V., Jaleta, M., Tesfaye, K., Abeyo, B., Devkota, M., Frija, A., Baudron, F., 2023. Pathways to wheat self-sufficiency in Africa. Glob. Food Sec. 37, 100684.
Simane, B., Tanner, D.G., Tarekegne, A.T., Taa, A., 1999. Agro-Ecological Decision Support Systems for Wheat Improvement in Ethiopia: Climatic Characterization and Clustering of Wheat Growing Regions.
Song, X.P., Huang, W., Hansen, M.C., Potapov, P., 2021. An evaluation of Landsat, Sentinel-2, Sentinel-1 and MODIS data for crop type mapping. Sci. Remote Sens. 3, 100018.
Stuart, A.M., Pame, A.R.P., Silva, J.V., Dikitanan, R.C., Rutsaert, P., Malabayabas, A.J.B., Lampayan, R.M., Radanielson, A.M., Singleton, G.R., 2016. Yield gaps in rice-based farming systems: insights from local studies and prospects for future analysis. Field Crop Res. 194, 43–56. https://doi.org/10.1016/j.fcr.2016.04.039.
Stutz, D., Hermans, A., Leibe, B., 2018. Superpixels: an evaluation of the state-of-the-art. Comput. Vis. Image Underst. 166, 1–27.
Tadesse, W., Zegeye, H., Debele, T., Kassa, D., Shiferaw, W., Solomon, T., Assefa, S., 2022. Wheat production and breeding in Ethiopia: retrospect and prospects. Crop Breed. Genet. Genom. 4 (3). https://doi.org/10.20900/cbgg20220003.
Tamene, L., Abera, W., Bendito, E., Erkossa, T., Tariku, M., Sewnet, H., Tibebe, D., Sied, J., Feyisa, G., Wondie, M., Tesfaye, K., 2022. Data-driven similar response units for agricultural technology targeting: an example from Ethiopia. Exp. Agric. 58, e27. https://doi.org/10.1017/S0014479722000126.
Tesfaye, K., Jaleta, M., Jena, P., Mutenje, M., 2015. Identifying potential recommendation domains for conservation agriculture in Ethiopia, Kenya, and Malawi. Environ. Manag. 55 (2), 330–346.
Tomasini, C., Emmendorfer, L., Borges, E.N., Machado, K., 2016. A methodology for selecting the most suitable cluster validation internal indices. In: Proceedings of the 31st Annual ACM Symposium on Applied Computing, pp. 901–903. https://doi.org/10.1145/2851613.2851885.
Trabucco, A., Zomer, R.J., 2018. Global aridity index and potential evapotranspiration (ET0) climate database v2. CGIAR Consort. Spat. Inf. 10, m9.
van Bussel, L.G.J., Grassini, P., Van Wart, J., Wolf, J., Claessens, L., Yang, H., Boogaard, H., de Groot, H., Saito, K., Cassman, K.G., van Ittersum, M.K., 2015. From field to atlas: upscaling of location-specific yield gap estimates. Field Crop Res. 177, 98–108. https://doi.org/10.1016/j.fcr.2015.03.005.
van Wart, J., van Bussel, L.G.J., Wolf, J., Licker, R., Grassini, P., Nelson, A., Boogaard, H., Gerber, J., Mueller, N.D., Claessens, L., van Ittersum, M.K., Cassman, K.G., 2013. Use of agro-climatic zones to upscale simulated crop yield potential. Field Crop Res. 143, 44–55. https://doi.org/10.1016/j.fcr.2012.11.023.
Vanlauwe, B., Tittonell, P., Mukalama, J., 2007. Within-farm soil fertility gradients affect the response of maize to fertilizer application in western Kenya. In: Bationo, A., Waswa, B., Kihara, J., Kimetu, J. (Eds.), Advances in Integrated Soil Fertility Management in Sub-Saharan Africa: Challenges and Opportunities. Springer, Netherlands, pp. 121–132. https://doi.org/10.1007/978-1-4020-5760-1_10.
Veldkamp, A., Kok, K., De Koning, G.H.J., Schoorl, J.M., Sonneveld, M.P.W., Verburg, P. H., 2001. Multi-scale system approaches in agronomic research at the landscape level. Soil Tillage Res. 58 (3), 129–140. https://doi.org/10.1016/S0167-1987(00)00163-X.
Walhazi, H., Maalej, A., Amara, N.E.B., 2024. A multi-classifier system for automatic fingerprint classification using transfer learning and majority voting. Multimed. Tools Appl. 83 (2), 6113–6136. https://doi.org/10.1007/s11042-023-15337-6.
White, J.W., Tanner, D.G., Corbett, J.D., 2001. An Agro-Climatological Characterization of Bread Wheat Production Areas in Ethiopia. https://doi.org/10.1016/j.agee.2007.06.006.
Williams, C.L., Hargrove, W.W., Liebman, M., James, D.E., 2008. Agro-ecoregionalization of Iowa using multivariate geographical clustering. Agric. Ecosyst. Environ. 123 (1), 161–174. https://doi.org/10.1016/j.agee.2007.06.006.
Wu, B., Zhang, M., Zeng, H., Tian, F., Potgieter, A.B., Qin, X., Loupian, E., 2023. Challenges and opportunities in remote sensing-based crop monitoring: a review. Natl. Sci. Rev. 10 (4), nwac290.
Xu, R., Wunsch, D., 2005. Survey of clustering algorithms. IEEE Trans. Neural Netw. 16 (3), 645–678. https://doi.org/10.1109/TNN.2005.845141.
You, L., Guo, Z., 2024. Spatial Allocation of Agricultural Production: IFPRI'S Latest SPAM2020.
You, L., Wood, S., Wood-Sichra, U., 2009. Generating plausible crop distribution maps for sub-Saharan Africa using a spatially disaggregated data fusion and optimization approach. Agric. Syst. 99 (2), 126–140. https://doi.org/10.1016/j.agsy.2008.11.003.
Zanaga, D., Van De Kerchove, R., Daems, D., De Keersmaecker, W., Brockmann, C., Kirches, G., Wevers, J., Cartus, O., Santoro, M., Fritz, S., Lesiv, M., Herold, M., Tsendbazar, N.-E., Xu, P., Ramoino, F., Arino, O., 2022. ESA WorldCover 10 m 2021 v200 (Version v200) [Data set]. Zenodo. https://doi.org/10.5281/zenodo.7254221.
Zhang, Y., Hepner, G.F., 2017. The dynamic-time-warping-based k-means++ clustering and its application in pheno-region delineation. Int. J. Remote Sens. 38 (6), 1720–1736. https://doi.org/10.1080/01431161.2017.1286055.